Prepared for submission to JCAP FERMILAB-PUB-23-807-T



# Unraveling TeV Halos with the Cherenkov Telescope Array

**Dan Hooper,**[a,b,c] **Elena Pinetti,**[a,b] **Anastasia Sokolenko**[a,b]

[a]Fermi National Accelerator Laboratory, Theoretical Astrophysics Department, Batavia, IL, 60510, USA

[b]University of Chicago, Kavli Institute for Cosmological Physics, Chicago, IL 60637, USA

[c]University of Chicago, Department of Astronomy & Astrophysics, Chicago, IL 60637, USA

**Abstract.** Pulsars are observed to emit bright and spatially extended emission at multi-TeV energies. Although such "TeV halos" appear to be an approximately universal feature of middle-aged pulsars, there remains much to be understood about these systems. In this paper, we project the ability of the Cherenkov Telescope Array (CTA) to measure the properties of TeV halos, focusing on the case of the nearby Geminga pulsar. We conclude that CTA will be able to provide important information about this source, allowing us to discriminate between a range of different models that are currently consistent with all existing data. In particular, such observations will help us to measure the normalization, energy dependence, and spatial dependence of the diffusion coefficient in the region that surrounds Geminga, as well as the spectrum of the electrons that are injected from this source.

## Contents


**1 Introduction** 1

**2 TeV-Scale Gamma Rays From Pulsars** 2

**3 The Cherenkov Telescope Array** 7

**4 Results** 9

**5 Summary and Conclusions** 10


## 1 Introduction

In 2017, the High-Altitude Water Cherenkov (HAWC) observatory reported the detection of bright and spatially extended multi-TeV emission from the regions surrounding the Geminga and Monogem pulsars [1, 2] (see also Ref. [3]). The spectrum and intensity of this emission reveal that these sources convert on the order of 10% of their total spin-down power into very high-energy electron-positron pairs. Furthermore, as each of these "TeV halos" is observed to extend out to $\sim 5^\circ$ in radius (corresponding to approximately $\sim 25\,\mathrm{pc}$), these observations indicate that cosmic rays propagate much less efficiently in the vicinity of these sources than they do elsewhere in the interstellar medium (ISM) [4–11].

Over the past few years, data from HAWC, HESS, and LHAASO has been used to identify TeV halos around many other middle-aged ($t_{\rm age} \sim 10^5 - 10^6\,\mathrm{yr}$) pulsars [12–21], supporting the conclusion that TeV halos are an approximately universal feature of such objects. In contrast, younger pulsars, such as the Crab ($t_{\rm age} \approx 964\,\mathrm{yr}$), have not been observed to produce extended multi-TeV emission [22–24]. These and other observations suggest that pulsars undergo several stages of evolution [25]. In the earliest of these stages ($t_{\rm age} \lesssim 10^4\,\mathrm{yr}$), electrons and positrons are confined within a so-called pulsar wind nebula. During this time, the powerful magnetic field of the neutron star accelerates charged particles which subsequently interact with the surrounding medium to create a termination shock. This shock leads to a second stage in which the shock fragments the pulsar wind nebula, allowing the cosmic rays to escape and propagate into the surrounding ISM. As an intermediate case, we note that the Vela pulsar ($t_{\rm age} \approx 11$ kyr) does not appear to have a typical TeV halo, but is surrounded by a $\sim 10$ pc region that produces significant emission in the GeV and radio bands [26–29]. Vela could thus potentially represent an example of a pulsar that is in a transition between its pulsar wind nebula and TeV halo stages [13].

Young neutron stars also generate significant gamma-ray emission as supernova remnants. Whereas both pulsar wind nebulae and TeV halos are powered by a pulsar's rotational kinetic energy, supernova remnants rely on the energy that is liberated in a supernova explosion. In contrast to pulsar wind nebulae and TeV halos, supernova remnants grow steadily, at a rate that depends on the density and other characteristics of the surrounding ISM. Such objects ultimately become much larger than either pulsar wind nebulae or TeV halos, with radii that extend out to $\sim 50-100\,\mathrm{pc}$ [30, 31]. Furthermore, while supernova remnants persist longer than pulsar wind nebulae, they are not nearly as long-lived as TeV halos. In particular,

supernova remnants become faint as their shocks slow down, typically on a timescale of tens of thousands of years [32].

As the very high-energy electrons and positrons accelerated by a pulsar diffuse away from their source and scatter with the radiation in the surrounding ISM, a TeV halo is formed. Geminga and Monogem are each prototypical examples of pulsars in this stage of evolution. The observed angular extent of TeV halos forces us to accept the puzzling fact that cosmic rays propagate in the vicinity of TeV halos much more slowly than they do elsewhere in the ISM [1, 2, 33, 34]. Furthermore, the intensity of the multi-TeV gamma-ray emission from these objects implies that a significant fraction of their pulsars' total spin-down power is being converted into the acceleration of very high-energy electrons and positrons. Among other implications, this supports the conclusion that pulsars are responsible for generating the cosmic-ray positron excess, as reported by the PAMELA and AMS-02 collaborations [4, 35–41] (see also Refs. [3, 42–46]).

Of the approximately 3400 pulsars that have been detected to date, the vast majority of these objects have been observed only at radio wavelengths [47, 48]. Such pulsars are characterised by their emission of pulsating electromagnetic radiation, which is visible only to an observer that is aligned along their magnetic axes. As a result, it is reasonable to conclude that most of the Milky Way's pulsars – those with radio beams that are *not* pointed in our direction – have not yet been detected. In contrast to their radio beams, the very high-energy emission associated with a pulsar's TeV halo is emitted isotropically. TeV halos thus represent a powerful means by which to discover pulsars whose radio beams are not aligned in our direction [12].

There remains much to understand about the physics of TeV halos. In particular, it is not yet known why or how the process of diffusion is inhibited in the volume surrounding these sources (for discussions, see Refs. [9, 10, 49–53]). To discriminate between various models that could potentially account for this observed behavior, it will be essential for us to measure the spectrum and angular distribution of the gamma-ray emission from TeV halos in much greater detail. Particularly promising in this regard is the upcoming Cherenkov Telescope Array (CTA), which will offer unprecedented angular resolution and overall sensitivity to gamma rays in the energy range of $E_\gamma \sim 10^2 - 10^5$ GeV. In this paper, we consider the ability of CTA to distinguish between different models of TeV halos, focusing on the specific case of Geminga. To this end, we consider a variety of models with different values for the parameters associated with the injected electron spectrum, the time evolution of the pulsar's spin-down, and the diffusion coefficient surrounding the pulsar. We identify a variety of models that are currently consistent with all existing data, but that could be differentiated by CTA.[1]

## 2 TeV-Scale Gamma Rays From Pulsars

The propagation and energy losses of electrons[2] can be described by the following transport equation:

$$\frac{\partial}{\partial t}\frac{\mathrm{d}n_e}{\mathrm{d}E_e}(E_e,\vec{r},t) - \vec{\nabla}\cdot\left[D(E_e,\vec{r})\,\vec{\nabla}\,\frac{\mathrm{d}n_e}{\mathrm{d}E_e}(E_e,\vec{r},t)\right] + \frac{\partial}{\partial E_e}\left[b_{\rm tot}(E_e)\frac{\mathrm{d}n_e}{\mathrm{d}E_e}(E_e,\vec{r},t)\right] = Q(E_e,\vec{r},t)\ ,$$

where $dn_e/dE_e$ is the differential number density of electrons, $D$ is the diffusion coefficient, and $b_{\rm tot}$ is the total energy loss rate from inverse Compton scattering and synchrotron emission.

[1] For a complementary study assessing the ability of CTA to study the characteristics of the Milky Way's TeV halo population, see Ref. [54].

[2] Throughout this paper, we will often refer to electrons and positrons simply as "electrons".

On the right-hand side, $Q$ is the injected spectrum, representing the source of the electrons in question.

We model a pulsar as a point source of energetic electrons and assume that the injected spectrum follows a power-law with an exponential cut-off [55], allowing us to write the source terms as follows:

$$Q(E_e, \vec{r}, t) = Q_\star \, E_e^{-\alpha} \, \exp\left(-\frac{E_e}{E_{\rm cut}}\right) \, L(t) \, \delta(\vec{r}) \, , \tag{2.1}$$

where $Q_\star$ is the normalization of the spectrum, $\alpha$ and $E_{\rm cut}$ are spectral index and cutoff of the injected electrons, and $L(t)$ accounts for the time dependence of the luminosity in injected electrons. We take the electron luminosity to be proportional to the rate at which the pulsar loses rotational kinetic energy (i.e., its spin-down power), which can be expressed as

$$L(t) = L_0 \left(1 + \frac{t}{\tau}\right)^{-\frac{n+1}{n-1}} \, , \tag{2.2}$$

where $L_0$ is the initial spin-down luminosity, $n$ the braking index, and $\tau$ is the characteristic spin-down timescale. While many pulsars exhibit breaking indices near $n = 3$ (corresponding to the case of magnetic dipole breaking), others evolve as rapidly as $n \sim 1.4$ [56]. We further introduce the quantity $\eta$, which is the fraction of a pulsar's total spin-down power that goes into the production of electron-positron pairs with $E_e > 0.1\,{\rm GeV}$, $L = \eta \dot{E}_{\rm rot}$.

In the energy range of interest, electrons lose energy through a combination of inverse Compton scattering and synchrotron radiation, $b_{\rm tot} = b_{\rm sync} + b_{\rm ICS}$ [57]. These contributions to the energy loss rate are given by

$$b_{\rm sync} = \frac{2\sigma_{\rm t} c B^2}{3 m_e^2 \mu_0} \left(\frac{E_e}{m_e}\right)^2 \, , \tag{2.3}$$

$$b_{\rm ICS} = \sum_i \frac{4\sigma_{\rm t} u_i \, S_i(E_e)}{3c^3} \left(\frac{E_e}{m_e}\right)^2 \, , \tag{2.4}$$

where $\sigma_{\rm t}$ is the Thomson cross-section, $\mu_0$ is the permeability constant, and we take the strength of the magnetic field to be $B = 3\,\mu G$. The sum in the expression for the inverse Compton losses runs over the different components of the interstellar radiation field, which we take to be the cosmic microwave background ($T_{\rm CMB} = 2.75$ K, $u_{\rm CMB} = 0.26$ eV/cm$^3$), infrared emission from dust ($T_{\rm IR} = 20$ K, $u_{\rm IR} = 0.60$ eV/cm$^3$), and optical starlight ($T_{\rm SL} = 5000$ K, $u_{\rm SL} = 0.60$ eV/cm$^3$) [4, 58, 59]. At very high energies, $E_e > m_e^2/2T$, inverse Compton scattering occurs in the Klein-Nishina regime, characterized by the following suppression factor:

$$S_i(E_e) = \frac{A_i}{A_i + (E_e/m_e)^2} \, , \tag{2.5}$$

where $A_i = 45 m_e^2 / 64\pi^2 T_i^2$.

For the diffusion coefficient, we consider in this study a two-zone model, in which we take the magnitude and energy dependence of the diffusion coefficient to change at a distance, $r_h$, from the pulsar,

$$D(E_e) = \begin{cases} D_0 \, (E_e/1\,{\rm GeV})^{\delta} & r \leq r_h \\ D_{\rm ISM} \, (E_e/1\,{\rm GeV})^{\delta_{\rm ISM}} & r > r_h \, . \end{cases} \tag{2.6}$$

The observed angular extent of TeV halos strongly favors two-zone models over those with a uniform diffusion coefficient. In particular, whereas diffusion in the ISM is characterized

by $D_{\rm ISM} \sim 4 \times 10^{28}\,{\rm cm}^2/{\rm s}$ and $\delta_{\rm ISM} \sim 1/3$ [60, 61], the observed morphology of the Geminga and Monogem halos each require $D_0 \sim 10^{26}\,{\rm cm}^2/{\rm s}$ (for $\delta = 1/3$) [4, 35, 36, 62, 63].

The diffusion coefficient and energy loss rates can be used together to determine the diffusion length, $\lambda$, over which electrons are typically displaced:

$$\lambda(E_e, E_0) = \left[ 4 \int_{E_0}^{E_e} {\rm d}E_e' \, \frac{D(E_e')}{b_{\rm tot}(E_e')} \right]^{1/2}, \tag{2.7}$$

where $E_0$ and $E_e$ are the initial and final electron energies, respectively. We can further relate these energies to the amount of time that has passed since the electrons were injected:

$$\int_{E_0}^{E_e} \frac{1}{b_{\rm tot}(E_e')} = t_\star \, , \tag{2.8}$$

where $t_\star \equiv t_{\rm obs} - t_{\rm inj}$ is the difference between the time of the observation and time at which the electrons were injected from the pulsar. This allows us to treat the diffusion length as a function of the final energy and the time since injection, $\lambda(E_e, t_\star)$. Note that if the diffusion coefficient in the region surrounding Geminga had been similar to that observed elsewhere in the ISM, the inverse Compton emission due to 35 TeV electrons, would extend out to a distance of $\lambda \sim 200\,{\rm pc}$, corresponding to an angular scale of $\sim 60^\circ$, far beyond the $\sim 2^\circ$ extension observed by HAWC and Milagro. It is this key observation that forces us to conclude that diffusion is very inefficient in the vicinity of these pulsars.

The distribution of the energetic electrons from a TeV halo can be expressed as

$$\frac{{\rm d}n_e}{{\rm d}E_e}(E_e, r, t) = \int_0^t \frac{dt'\, Q_\star\, L(t')\, E_0\, (E_e, t-t')^{2-\alpha}}{\pi^{3/2}\, E_e^2\, \lambda(E_e, t-t')^3} \exp\left[ - \frac{E_0(E_e, t-t')}{E_{\rm cut}} \right] \exp\left[ - \left( \frac{r}{\lambda(E_e, t-t')} \right)^2 \right], \tag{2.9}$$

where $E_0$ is evaluated using Eq. (2.8) with $t_\star = t - t'$. Keep in mind that both $E_0$ and $\lambda$ are functions of $E_e$.

The second element that we will need in order to compute the gamma-ray flux from a TeV halo is the spectrum of inverse Compton emission that is produced by a given high-energy electron. The differential spectrum of inverse Compton emission radiated from an electron of energy $E_e$ is given by [55, 57, 64]

$$\frac{dN_\gamma}{dE_\gamma}(E_\gamma, E_e) = c \int d\epsilon \frac{dn}{d\epsilon}(\epsilon)\, \frac{d\sigma_{\rm ICS}}{dE_\gamma}(E_\gamma, \epsilon, E_e), \tag{2.10}$$

where $d\sigma_{\rm ICS}/dE_\gamma$ is the differential cross section for inverse Compton scattering [65] and $dn/d\epsilon$ is the differential number density of target radiation. We take this radiation to consist of a sum of blackbodies associated with the cosmic microwave background, infrared emission from dust, and starlight, with energy densities and temperatures as described earlier in this section.

To obtain the flux of photons that reach Earth, we convolve the electron density with the spectrum of inverse Compton emission per electron,

$$\frac{d\phi_\gamma}{dE_\gamma}(E_\gamma) = \int d\phi \int d\theta \sin\theta \int_{los} ds \int dE_e \, \frac{dn_e}{dE_e}(E_e, \vec{r}\,)\, \frac{dN_\gamma}{dE_\gamma}(E_\gamma, E_e), \tag{2.11}$$

where $s$ is the path along the line-of-sight ($los$).

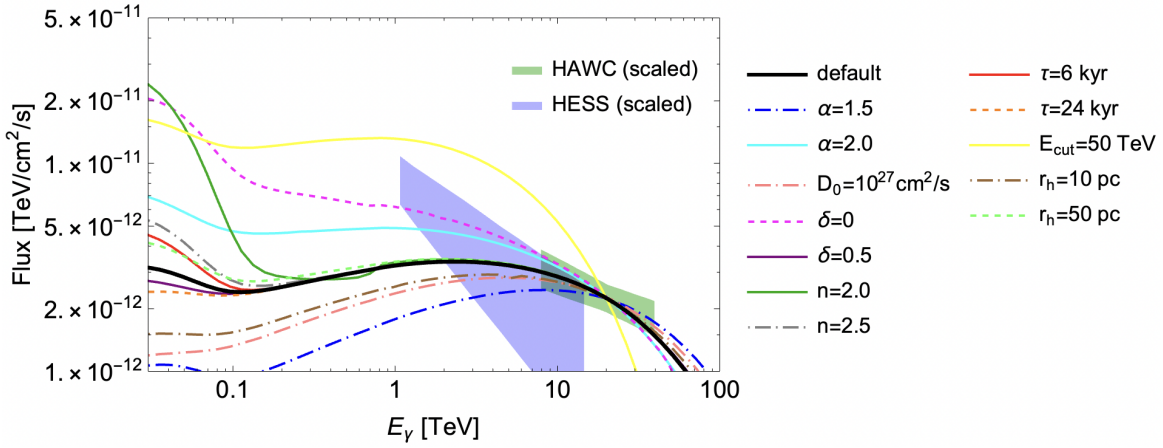


**Figure 1**. The impact of various parameters on the spectrum of the gamma-ray emission from a Geminga-like TeV halo, as integrated within a 2.5° radius. These predictions are compared to Geminga's spectrum, as measured by HAWC [1] and HESS [66]. For our default parameters, we have adopted $\alpha = 1.8$, $D_0 = 10^{26}\,\mathrm{cm}^2/\mathrm{s}$, $\delta = 0.33$, $n = 3.0$, $r_h = 30\,\mathrm{pc}$, $\tau = 12\,\mathrm{kyr}$, $E_{\rm cut} = 500\,\mathrm{TeV}$, and $\eta = 0.25$. Each curve is normalized to the measured flux at $E_\gamma = 20\,\mathrm{TeV}$.

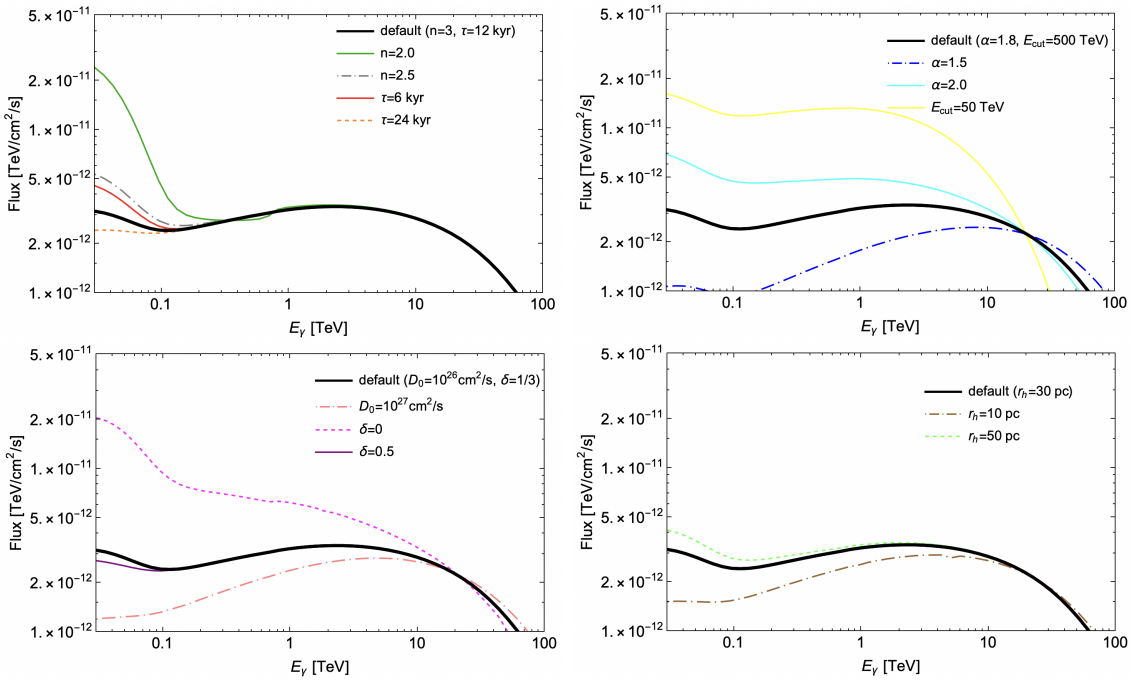


**Figure 2**. As in Fig. 1, but showing the impact of different parameters in separate frames for clarity.

In Figs. 1 and 2, we show the impact of the various parameters described in this section on the spectrum of the gamma-ray emission from a Geminga-like TeV halo. For our default parameters, we have adopted $\alpha = 1.8$, $D_0 = 10^{26}\,\mathrm{cm}^2/\mathrm{s}$, $\delta = 0.33$, $n = 3.0$, $r_h = 30\,\mathrm{pc}$, $\tau = 12\,\mathrm{kyr}$, $E_{\rm cut} = 500\,\mathrm{TeV}$, and $\eta = 0.25$. Each curve in this figure (and throughout this paper) is normalized such that it has the same flux at $E_\gamma = 20\,\mathrm{TeV}$ (see Table 2 for the required efficiencies, $\eta$). We take the distance to Geminga to be 250 pc and its age to be

| Model Name | Efficiency, $\eta$ |
|---|---|
| Default | 28% |
| $n = 2.0$ | 28% |
| $n = 2.5$ | 28% |
| $\tau = 6\,\mathrm{kyr}$ | 28% |
| $\tau = 24\,\mathrm{kyr}$ | 28% |
| $D_0 = 10^{27}\,\mathrm{cm}^2/\mathrm{s}$ | 130% |
| $\delta = 0$ | 14% |
| $\delta = 0.5$ | 94% |
| $\alpha = 1.5$ | 17% |
| $\alpha = 2.0$ | 71% |
| $E_{\mathrm{cut}} = 50\,\mathrm{TeV}$ | 97% |
| $r_h = 10\,\mathrm{pc}$ | 43% |
| $r_h = 50\,\mathrm{pc}$ | 28% |

**Table 1**. The efficiencies, $\eta$, adopted for TeV halo models used in this study. Our default model corresponds to $n = 3.0$, $\tau = 12\,\mathrm{kyr}$, $\alpha = 1.8$, $E_{\mathrm{cut}} = 500\,\mathrm{TeV}$, $D_0 = 10^{26}\,\mathrm{cm}^2/\mathrm{s}$, $\delta = 0.33$, and $r_h = 30\,\mathrm{pc}$.

340 kyr.

In the upper left frame of Fig. 2, we illustrate how the pulsar braking index, $n$, and the pulsar's spin-down timescale, $\tau$, each impact the shape of the gamma-ray spectrum. At high energies ($E_\gamma \gtrsim 0.3\,\mathrm{TeV}$), these parameters do not significant impact the spectrum. This is because photons in this energy range are produced by very high-energy electrons which lose energy on a timescale that is much shorter than the age of the pulsar or the time that would be required for those particles to escape from the halo. The observed gamma-ray spectrum thus reflects the current injection rate of very high-energy electrons. At lower energies, in contrast, the values of $n$ and $\tau$ can each significantly impact the predicted spectrum.

In the lower left frame of Fig. 2, we show how the diffusion parameters, $D_0$ and $\delta$, impact the predicted spectrum. Again, these parameters do not significantly impact the spectrum at the highest energies ($E_\gamma \gtrsim 10\,\mathrm{TeV}$), but do at lower energies, where the timescale for electrons to escape the halo becomes comparable to the age of the pulsar. Note that the $D_0 = 10^{27}\,\mathrm{cm}^2/\mathrm{s}$ case requires an unphysical value of the efficiency, $\eta = 1.3$, and is only shown for illustration. In the upper right frame of the same figure, we show the impact of changes to the spectrum of injected electrons, as parameterized by $\alpha$ and $E_{\mathrm{cut}}$. Lastly, in the lower right frame of this figure, we show the impact of the radius of the TeV halo, $r_h$ (beyond which the diffusion coefficient takes on standard ISM values).

In Figs. 3, 4, and 5, we illustrate the impact of these same parameters on the surface brightness profile of the gamma-ray emission from a Geminga-like TeV halo. These results are shown as integrated over two ranges of energy: 0.3 to 3 TeV (as could be measured by CTA) and 8 to 40 TeV (as has been measured by HAWC [1]). From the upper left frames of Figs. 4 and 5 we see that the pulsar braking index, $n$, and pulsar spin-down timescale, $\tau$, have little impact on the predicted surface brightness profile. These measurements, however, are much more sensitive to the other parameters considered in this study. Note that some of these parameters can impact the predicted angular distribution in different ways over different ranges of energy, making the results of HAWC and CTA highly complementary. For example,

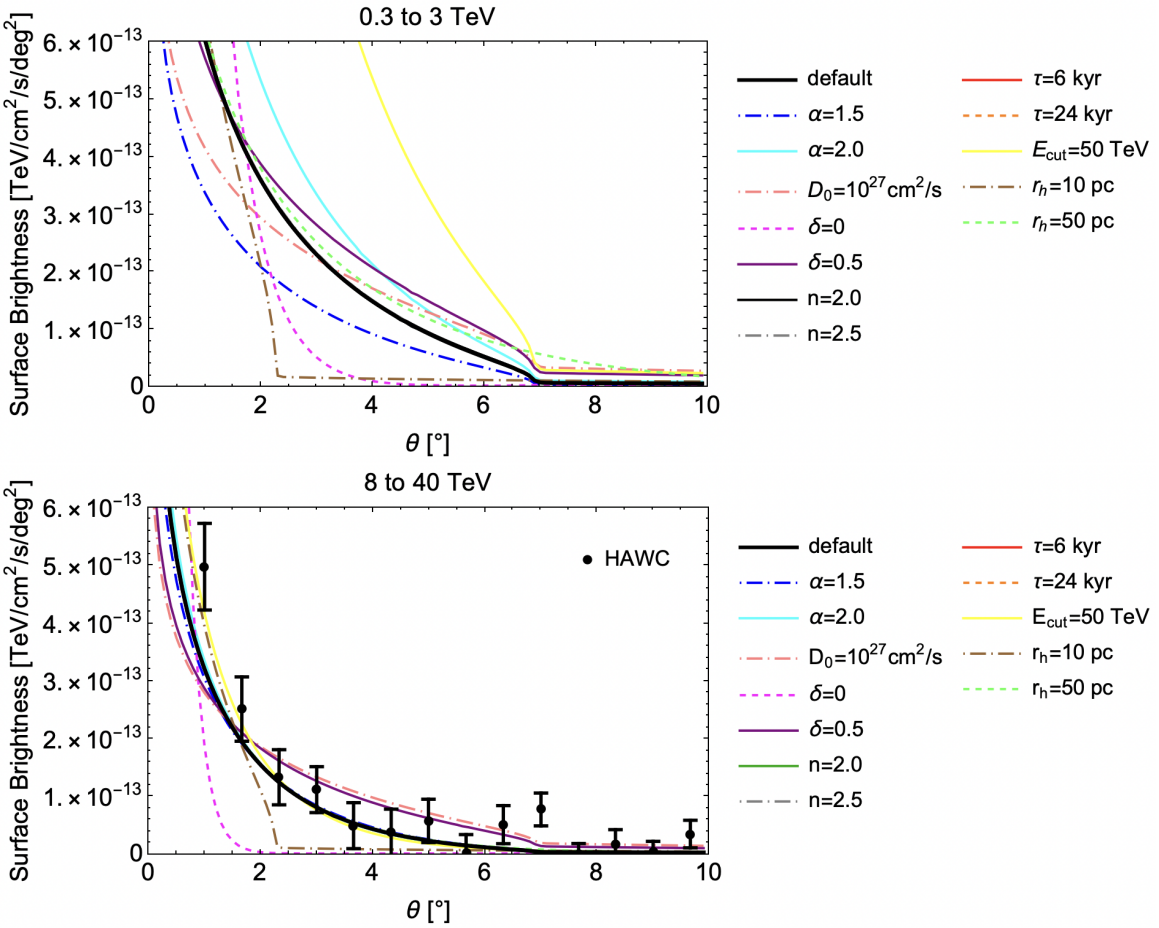


**Figure 3**. The impact of various parameters on the surface brightness profile of the gamma-ray emission from a Geminga-like TeV halo, integrated over two ranges of energy. The predictions for the 8-40 TeV case are compared in the lower frame to the measurements of HAWC [1]. For our default parameters, we have adopted $\alpha = 1.8$, $D_0 = 10^{26}\,\mathrm{cm}^2/\mathrm{s}$, $\delta = 0.33$, $n = 3.0$, $r_h = 30\,\mathrm{pc}$, $\tau = 12\,\mathrm{kyr}$, $E_{\rm cut} = 500\,\mathrm{TeV}$, and $\eta = 0.25$. Each curve is normalized such that it has the measured flux at $E_\gamma = 20\,\mathrm{TeV}$.

notice that although the different choices of $\alpha$ and $E_{\rm cut}$ considered here only modestly impact the surface brightness profile at HAWC energies, these parameters have a greater impact in the energy range that will be measured by CTA.

## 3 The Cherenkov Telescope Array

The Cherenkov Telescope Array (CTA) will be the flagship of the next-generation instruments in the field of gamma-ray astronomy. It will cover an extensive energy range from 20 GeV to 300 TeV with an energy resolution better than 10%, and with much greater angular resolution than existing gamma-ray telescopes [67]. CTA will include two different telescope arrays; one in each hemisphere. CTA North will consist of 4 large (23 m diameter) and 9 medium sized (12 m diameter) telescopes. In contrast, CTA South will consist of 4 large and 14 medium sized telescopes, along with 37 smaller (4 m) telescopes.

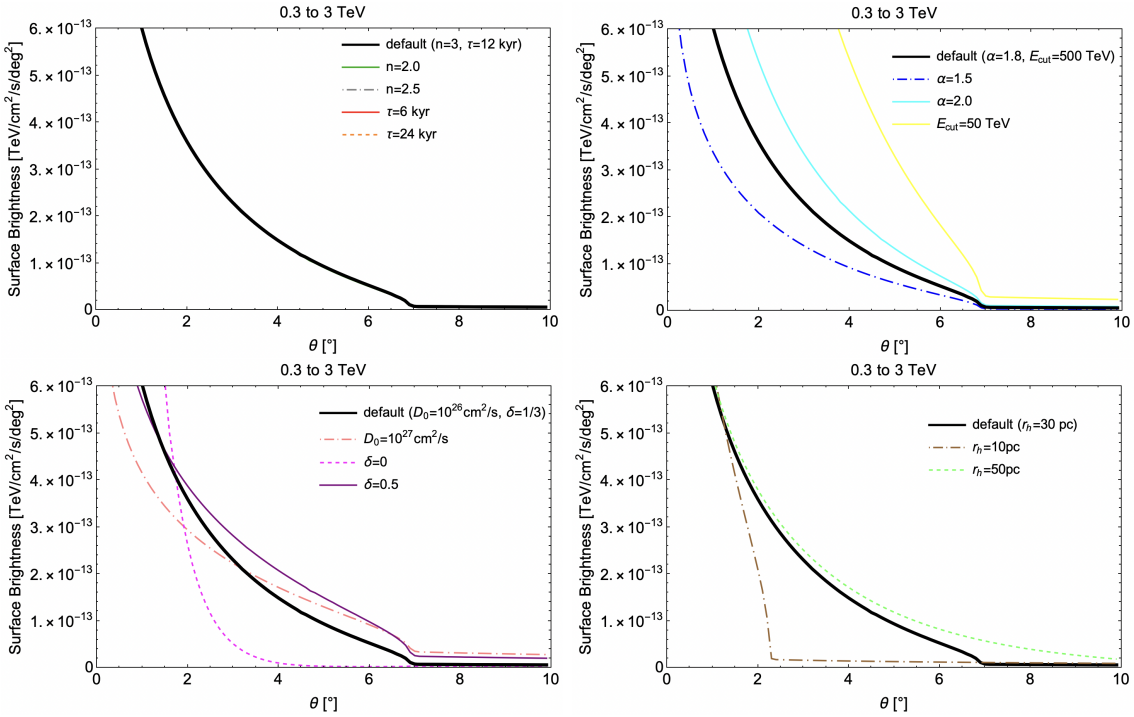


**Figure 4**. As in Fig. 3, but showing the impact of different parameters in separate frames for clarity.

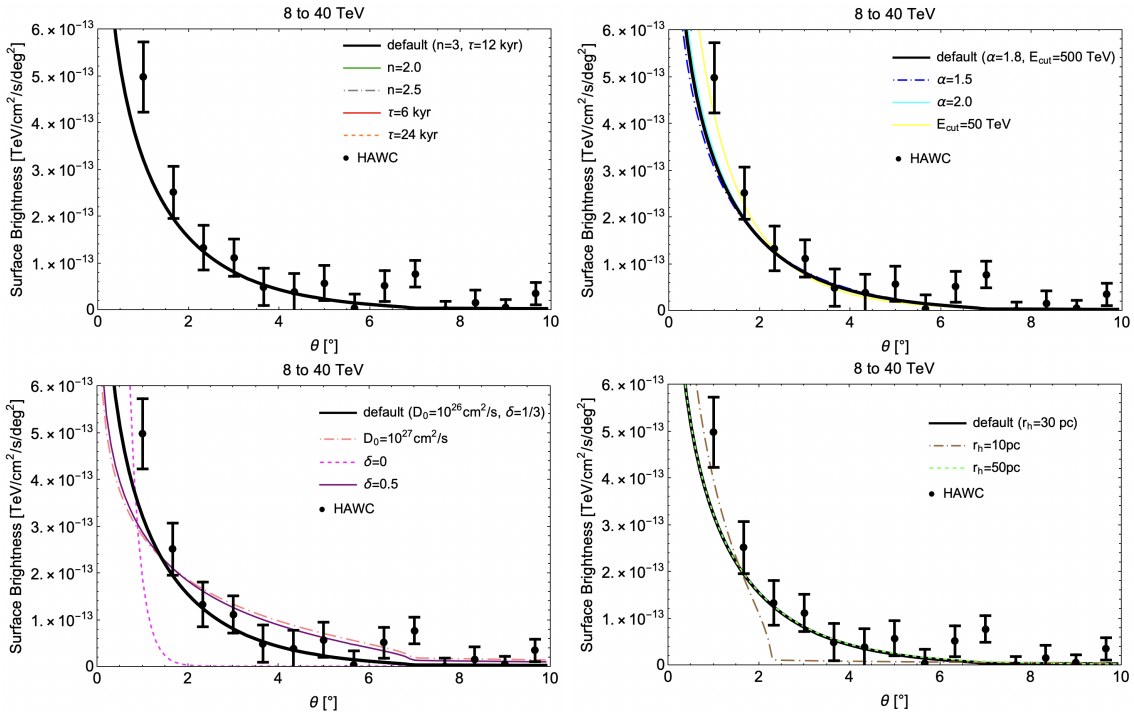


**Figure 5**. As in Fig. 3, but showing the impact of different parameters in separate frames for clarity.

To assess CTA's ability to distinguish between different models of TeV halos, we have made use of the publicly available code *gammapy* [68] and have adopted the *prod5* instrument

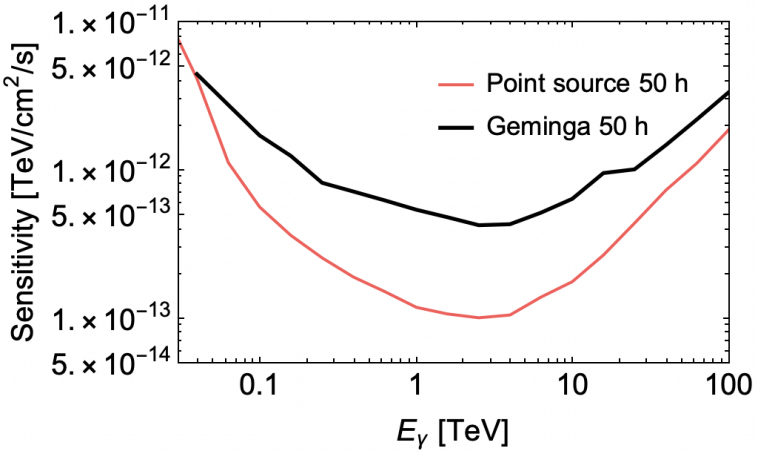


**Figure 6**. The $5\sigma$ sensitivity of CTA North to a source with an angular extent equal to that of Geminga's TeV halo (adopting our default parameters), after 50 hours of observation. This sensitivity was calculated independently in each of 20 energy bins. For comparison, we also show the analogous sensitivity of CTA to a point source [70].

response function (specifically, *North-20deg-AverageAz-4LSTs09MSTs.180000s-v0.1*). Using this software, we simulated mock data for each model of Geminga's TeV halo, considering a total of 50 hours of observation by CTA North. We have taken CTA's field-of-view to be a $5^\circ \times 5^\circ$ region centered on Geminga and have divided the data into $0.05^\circ \times 0.05^\circ$ angular bins, as well as 20 energy bins distributed logarithmically between 0.03 and 100 TeV. Each simulation incorporates both signal and background photons, utilizing the standard background model, *FoVBackgroundModel*, which employs modern models for the isotropic and Galactic diffuse emission [69].

In Fig. 6, we show the $5\sigma$ sensitivity of CTA North to a source with an angular extent equal to that of Geminga's TeV halo (adopting our default parameters), after 50 hours of observation. This sensitivity was calculated independently in each of 20 energy bins. For comparison, we also show the analogous sensitivity of CTA to a point source. The extended nature of Geminga's TeV halo non-negligibly reduces CTA's sensitivity.

## 4 Results

In this section, we project the ability of CTA to test and discriminate between various models of TeV halos, using the Geminga TeV halo as a case study. To this end, we utilize the simulation described in the previous section to calculate the predicted flux in each bin for a given model. We then compute the expected error bars around this flux, $\Delta F = F \times (\Delta N / N_S)$, where $\Delta N = \sqrt{N_S + N_{BG}}$, $N_S$ is the predicted number of signal events, and $N_{BG}$ is the predicted number of background events.

Our results as they pertain to the energy spectrum of Geminga are shown in Fig. 7, where the shaded band reflects our projection for CTA's uncertainties, as calculated (at the $1\sigma$ level) independently in each energy bin, and adopting the case of our default TeV halo model. A casual inspection of this figure reveals that CTA will be able to differentiate our default model of Geminga's TeV halo from models with a relatively low energy cut off ($E_{\rm min} = 50\,{\rm TeV}$), or that feature energy-independent diffusion ($\delta = 0$). CTA will also be able to infer the injected spectral index of electrons, easily distinguishing between models with $\alpha = 2.0$, 1.8 or 1.5.

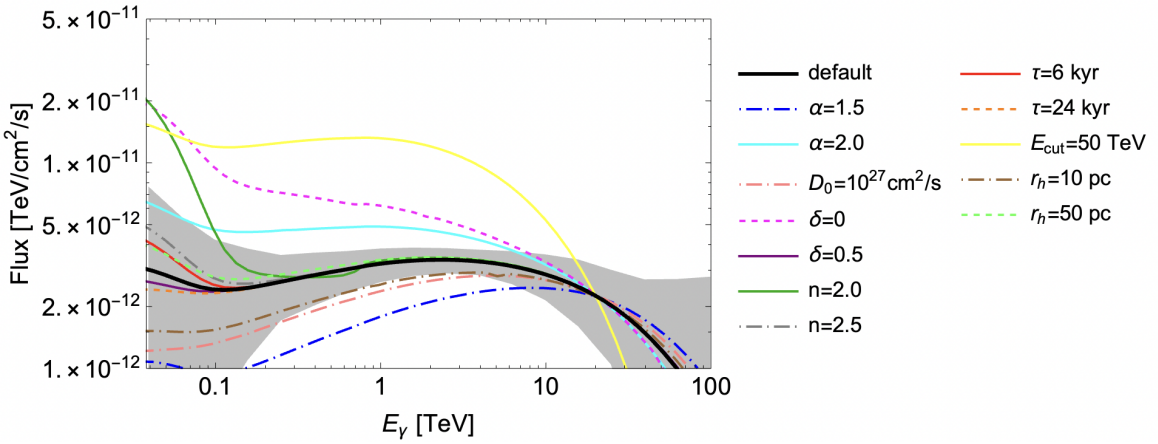


**Figure 7**. As in Fig. 1, with the shaded grey region representing the projected $1\sigma$ uncertainties after 50 hours of observation of the Geminga TeV halo with CTA North, for the case of our default model.

CTA should also be able to test models with a small halo radius ($r_h = 10\,\mathrm{pc}$), or with a larger diffusion coefficient than adopted in our default model ($D_0 = 10^{27}\,\mathrm{cm}^2/\mathrm{s}$). In contrast, this spectral information will not be able to discriminate our default model from models with $\delta = 0.5$, or be very sensitive to the values of $\tau$ or $n$.

In Fig. 8, we forecast the statistical significance at which CTA will be able to distinguish between different models of Geminga's TeV halo, assuming 50 hours of observation. Taking a given model to be the "true model" of Geminga's TeV halo (shown on the $x$-axis), we calculate the reduced $\chi^2$ of the fit for each of the models considered in this study (shown on the $y$-axis). Each reduced $\chi^2$ is then converted into a $p$-value and then into a statistical significance. Models that can be distinguished at the level of $5\sigma$ or more are shown in red, while other combinations are shown in grey. Note that these results take into account both spectral and spatial information, allowing us to differentiate between models that the measured spectrum alone would not be able to distinguish.

## 5 Summary and Conclusions

Observations by HAWC, LHAASO, and HESS have revealed the presence of bright and spatially extended multi-TeV emission from the regions surrounding many pulsars, including the nearby examples of Geminga and Monogem. The characteristics of this emission indicate that these sources convert on the order of 10% of their total spin-down power into very high-energy electrons and positrons which then generate the observed gamma rays through inverse Compton scattering. Surprisingly, the gamma-ray emission from TeV halos is observed to extend out to tens of parsecs in radius, requiring that cosmic rays propagate much less efficiently in the vicinity of these sources than they do elsewhere in the interstellar medium (ISM). How and why diffusion is inhibited within these regions remains an open question. To test and differentiate between different models which could potentially account for these observations will require more detailed measurements of the spectrum and morphology of the gamma-ray emission from these sources.

In this paper, we have studied the ability of the Cherenkov Telescope Array (CTA) to study the properties of TeV halos, focusing on the prototypical example of Geminga. We have considered a variety of models with different values for the parameters associated with the

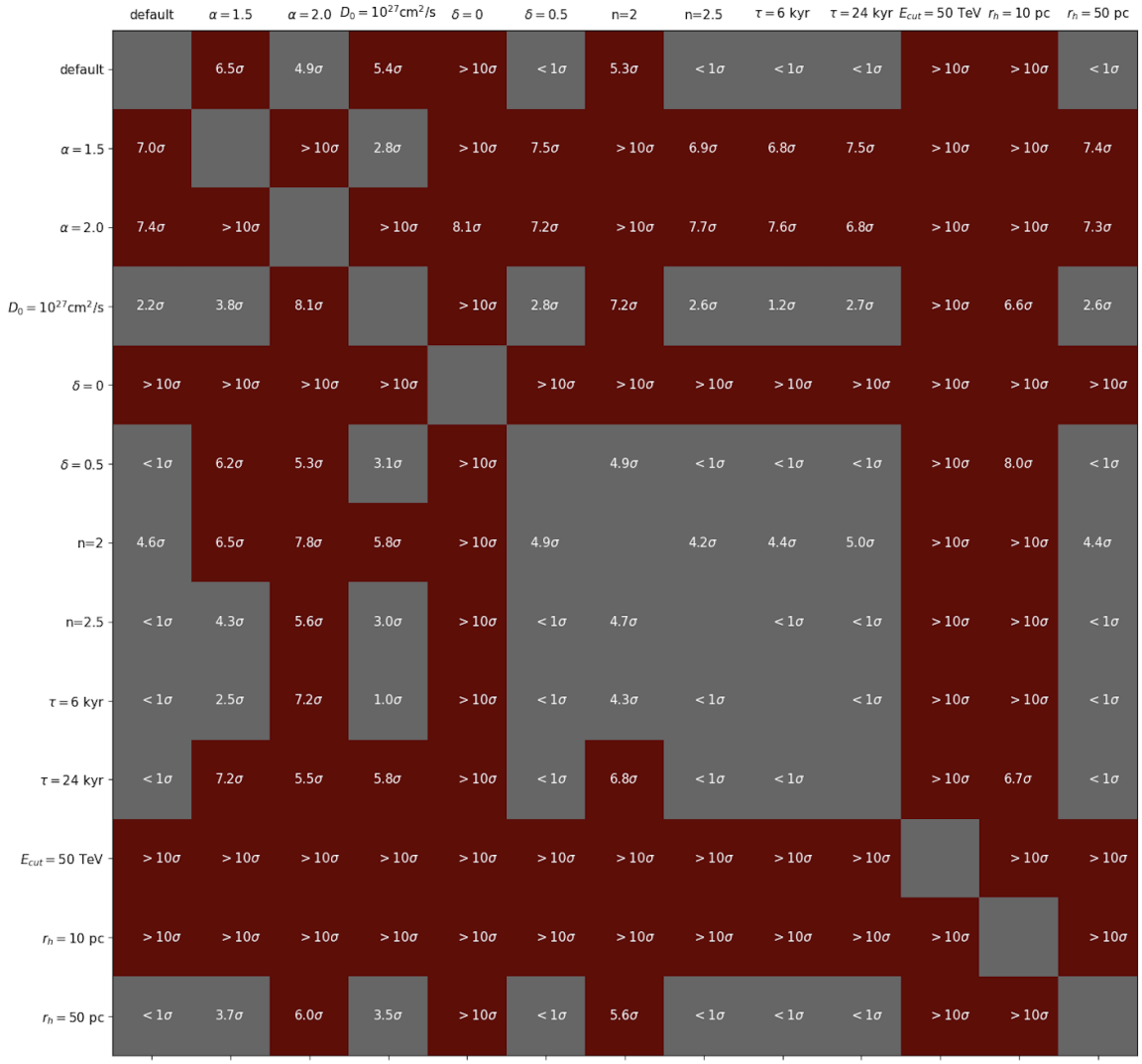


**Figure 8**. The statistical significance at which CTA is projected to be able to distinguish between different models for Geminga's TeV halo, after 50 hours of observation. Taking a given model to be the "true model" of Geminga's TeV halo (shown on the $x$-axis), we calculate the quality of the fit for each of the models considered in this study (shown on the $y$-axis). This information is then converted into the number of standard deviations at which the two models can be distinguished. Models that can be distinguished at the level of $5\sigma$ or more are shown in red, while other combinations are shown in grey.

injected electron spectrum, the time evolution of the pulsar's spin-down, and that describe the process of diffusion in the region surrounding the pulsar. We have identified many models that are consistent with all existing data, but that we project could be differentiated by CTA (see Figs. 7 and 8)

## Acknowledgments

We would like to thank Ilias Cholis, Luca Orusa, Ievgen Vovk, Igor Moskalenko, Volodymyr Savchenko and Vadym Voitsekhovskyi for helpful discussions. We acknowledge support from

*Fermi Research Alliance, LLC* under Contract No. DE-AC02-07CH11359 with the U.S. Department of Energy, Office of High Energy Physics.

## References


[1] HAWC collaboration, *Extended gamma-ray sources around pulsars constrain the origin of the positron flux at Earth*, *Science* **358** (2017) 911 [1711.06223].

[2] A.U. Abeysekara et al., *The 2HWC HAWC Observatory Gamma Ray Catalog*, *Astrophys. J.* **843** (2017) 40 [1702.02992].

[3] A.A. Abdo et al., *Milagro Observations of TeV Emission from Galactic Sources in the Fermi Bright Source List*, *Astrophys. J. Lett.* **700** (2009) L127 [0904.1018].

[4] D. Hooper, I. Cholis, T. Linden and K. Fang, *HAWC observations strongly favor pulsar interpretations of the cosmic-ray positron excess*, *Physical Review D* **96** (2017) .

[5] R.N. Manchester, G.B. Hobbs, A. Teoh and M. Hobbs, *VizieR Online Data Catalog: ATNF Pulsar Catalog (Manchester+, 2005)*, *VizieR Online Data Catalog* (2005) VII/245.

[6] R. López-Coto and G. Giacinti, *Constraining the properties of the magnetic turbulence in the Geminga region using HAWC $\gamma$-ray data*, *Mon. Not. Roy. Astron. Soc.* **479** (2018) 4526 [1712.04373].

[7] G. Johannesson, T.A. Porter and I.V. Moskalenko, *Cosmic-Ray Propagation in Light of the Recent Observation of Geminga*, *Astrophys. J.* **879** (2019) 91 [1903.05509].

[8] M. Di Mauro, S. Manconi and F. Donato, *Evidences of low-diffusion bubbles around Galactic pulsars*, *Phys. Rev. D* **101** (2020) 103035 [1908.03216].

[9] C. Evoli, T. Linden and G. Morlino, *Self-generated cosmic-ray confinement in TeV halos: Implications for TeV $\gamma$-ray emission and the positron excess*, *Phys. Rev. D* **98** (2018) 063017 [1807.09263].

[10] K. Fang, X.-J. Bi and P.-F. Yin, *Possible origin of the slow-diffusion region around Geminga*, *Mon. Not. Roy. Astron. Soc.* **488** (2019) 4074 [1903.06421].

[11] D. Hooper and T. Linden, *Evidence of TeV halos around millisecond pulsars*, *Phys. Rev. D* **105** (2022) 103013 [2104.00014].

[12] T. Linden, K. Auchettl, J. Bramante, I. Cholis, K. Fang, D. Hooper et al., *Using HAWC to discover invisible pulsars*, *Phys. Rev. D* **96** (2017) 103016 [1703.09704].

[13] T. Sudoh, T. Linden and J.F. Beacom, *TeV Halos are Everywhere: Prospects for New Discoveries*, *Phys. Rev. D* **100** (2019) 043016 [1902.08203].

[14] T. Sudoh, T. Linden and D. Hooper, *The Highest Energy HAWC Sources are Likely Leptonic and Powered by Pulsars*, *JCAP* **08** (2021) 010 [2101.11026].

[15] HAWC collaboration, *3HWC: The Third HAWC Catalog of Very-High-Energy Gamma-ray Sources*, *Astrophys. J.* **905** (2020) 76 [2007.08582].

[16] A. Smith, *A Systematic Search for TeV Halos associated with known pulsars*, in *36th International Cosmic Ray Conference (ICRC2019)*, vol. 36 of *International Cosmic Ray Conference*, p. 797, July, 2019, DOI.

[17] HESS collaboration, *The H.E.S.S. Galactic plane survey*, *Astron. Astrophys.* **612** (2018) A1 [1804.02432].

[18] HESS collaboration, *The population of TeV pulsar wind nebulae in the H.E.S.S. Galactic Plane Survey*, *Astron. Astrophys.* **612** (2018) A2 [1702.08280].

[19] LHAASO collaboration, *The First LHAASO Catalog of Gamma-Ray Sources*, 2305.17030.

[20] LHAASO collaboration, *Extended Very-High-Energy Gamma-Ray Emission Surrounding PSR J0622+3749 Observed by LHAASO-KM2A*, *Phys. Rev. Lett.* **126** (2021) 241103 [2106.09396].

[21] K. Fang, S.-Q. Xi and X.-J. Bi, *Self-consistent interpretations of the multiwavelength gamma-ray spectrum of LHAASO J0621+3755*, *Phys. Rev. D* **104** (2021) 103024 [2107.02140].

[22] F. Aharonian, A.G. Akhperjanian, A.R. Bazer-Bachi, M. Beilicke, W. Benbow, D. Berge et al., *Observations of the crab nebula with HESS*, *Astronomy & Astrophysics* **457** (2006) 899.

[23] J. Albert, E. Aliu, H. Anderhub, P. Antoranz, A. Armada, C. Baixeras et al., *VHE γ-ray observation of the crab nebula and its pulsar with the MAGIC telescope*, *The Astrophysical Journal* **674** (2008) 1037.

[24] A.U. Abeysekara, A. Albert, R. Alfaro, C. Alvarez, J.D. Á lvarez, R. Arceo et al., *Observation of the crab nebula with the HAWC gamma-ray observatory*, *The Astrophysical Journal* **843** (2017) 39.

[25] R.-Y. Liu, *The physics of pulsar halos: Research progress and prospect*, *Int. J. Mod. Phys. A* **37** (2022) 2230011 [2207.04011].

[26] A.A. Abdo, M. Ackermann, M. Ajello, A. Allafort, L. Baldini, J. Ballet et al., *FERMI LARGE AREA TELESCOPE OBSERVATIONS OF THE VELA-x PULSAR WIND NEBULA*, *The Astrophysical Journal* **713** (2010) 146.

[27] A. Abramowski, F. Acero, F. Aharonian, A.G. Akhperjanian, G. Anton, S. Balenderan et al., *Probing the extent of the non-thermal emission from the vela-x region at tev energies with h.e.s.s.*, *Astronomy & Astrophysics* **548** (2012) A38.

[28] M.-H. Grondin, R.W. Romani, M. Lemoine-Goumard, L. Guillemot, A.K. Harding and T. Reposeur, *THE VELA-x PULSAR WIND NEBULA REVISITED WITH FOUR YEARS FERMI LARGE AREA TELESCOPE OBSERVATIONS*, *The Astrophysical Journal* **774** (2013) 110.

[29] L. Tibaldo, R. Zanin, G. Faggioli, J. Ballet, M.-H. Grondin, J.A. Hinton et al., *Disentangling multiple high-energy emission components in the vela x pulsar wind nebula with the fermi large area telescope*, *Astronomy & Astrophysics* **617** (2018) A78.

[30] S.-Q. Xi, R.-Y. Liu, Z.-Q. Huang, K. Fang and X.-Y. Wang, *GeV observations of the extended pulsar wind nebulae constrain the pulsar interpretations of the cosmic-ray positron excess*, *Astrophys. J.* **878** (2019) 104 [1810.10928].

[31] J.N. Stafford, L.A. Lopez, K. Auchettl and T. Holland-Ashford, *The Age Evolution of the Radio Morphology of Supernova Remnants*, 1808.08234.

[32] S.K. Sarbadhicary, C. Badenes, L. Chomiuk, D. Caprioli and D. Huizenga, *Supernova Remnants in the Local Group I: A model for the radio luminosity function and visibility times of supernova remnants*, *Mon. Not. Roy. Astron. Soc.* **464** (2017) 2326 [1605.04923].

[33] R. Kappl, A. Reinert and M.W. Winkler, *AMS-02 Antiprotons Reloaded*, *JCAP* **10** (2015) 034 [1506.04145].

[34] Y. Génolini et al., *Cosmic-ray transport from AMS-02 boron to carbon ratio data: Benchmark models and interpretation*, *Phys. Rev. D* **99** (2019) 123028 [1904.08917].

[35] S. Profumo, J. Reynoso-Cordova, N. Kaaz and M. Silverman, *Lessons from HAWC pulsar wind nebulae observations: The diffusion constant is not a constant; pulsars remain the likeliest sources of the anomalous positron fraction; cosmic rays are trapped for long periods of time in pockets of inefficient diffusion*, *Physical Review D* **97** (2018) .

[36] K. Fang, X.-J. Bi, P.-F. Yin and Q. Yuan, *Two-zone diffusion of electrons and positrons from geminga explains the positron anomaly*, *The Astrophysical Journal* **863** (2018) 30.

[37] M. Di Mauro, F. Donato and S. Manconi, *Novel interpretation of the latest AMS-02 cosmic-ray electron spectrum*, *Phys. Rev. D* **104** (2021) 083012 [2010.13825].

[38] C. Evoli, E. Amato, P. Blasi and R. Aloisio, *Galactic factories of cosmic-ray electrons and positrons*, *Phys. Rev. D* **103** (2021) 083010 [2010.11955].

[39] S. Manconi, M. Di Mauro and F. Donato, *Contribution of pulsars to cosmic-ray positrons in light of recent observation of inverse-Compton halos*, *Phys. Rev. D* **102** (2020) 023015 [2001.09985].

[40] L. Orusa, S. Manconi, F. Donato and M. Di Mauro, *Constraining positron emission from pulsar populations with AMS-02 data*, *JCAP* **12** (2021) 014 [2107.06300].

[41] O.M. Bitter and D. Hooper, *Constraining the local pulsar population with the cosmic-ray positron fraction*, *JCAP* **10** (2022) 081 [2205.05200].

[42] D. Hooper, P. Blasi and P.D. Serpico, *Pulsars as the Sources of High Energy Cosmic Ray Positrons*, *JCAP* **01** (2009) 025 [0810.1527].

[43] H. Yuksel, M.D. Kistler and T. Stanev, *TeV Gamma Rays from Geminga and the Origin of the GeV Positron Excess*, *Phys. Rev. Lett.* **103** (2009) 051101 [0810.2784].

[44] D. Malyshev, I. Cholis and J. Gelfand, *Pulsars versus Dark Matter Interpretation of ATIC/PAMELA*, *Phys. Rev. D* **80** (2009) 063005 [0903.1310].

[45] M. Di Mauro, F. Donato, N. Fornengo, R. Lineros and A. Vittino, *Interpretation of AMS-02 electrons and positrons data*, *JCAP* **04** (2014) 006 [1402.0321].

[46] M. Boudaud et al., *A new look at the cosmic ray positron fraction*, *Astron. Astrophys.* **575** (2015) A67 [1410.3799].

[47] R.N. Manchester, G.B. Hobbs, A. Teoh and M. Hobbs, *The Australia Telescope National Facility pulsar catalogue*, *Astron. J.* **129** (2005) 1993 [astro-ph/0412641].

[48] Australian Telescope National Facility (ATNF) Pulsar Catalogue. https://www.atnf.csiro.au/people/pulsar/psrcat/.

[49] P. Mukhopadhyay and T. Linden, *Self-generated cosmic-ray turbulence can explain the morphology of TeV halos*, *Phys. Rev. D* **105** (2022) 123008 [2111.01143].

[50] P. De La Torre Luque, O. Fornieri and T. Linden, *Anisotropic diffusion cannot explain TeV halo observations*, *Phys. Rev. D* **106** (2022) 123033 [2205.08544].

[51] R.-Y. Liu, H. Yan and H. Zhang, *Understanding the Multiwavelength Observation of Geminga's Tev Halo: The Role of Anisotropic Diffusion of Particles*, *Phys. Rev. Lett.* **123** (2019) 221103 [1904.11536].

[52] S. Recchia, M. Di Mauro, F.A. Aharonian, L. Orusa, F. Donato, S. Gabici et al., *Do the Geminga, Monogem and PSR J0622+3749 $\gamma$-ray halos imply slow diffusion around pulsars?*, *Phys. Rev. D* **104** (2021) 123017 [2106.02275].

[53] L.-Z. Bao, K. Fang, X.-J. Bi and S.-H. Wang, *Slow Diffusion is Necessary to Explain the $\gamma$-Ray Pulsar Halos*, *Astrophys. J.* **936** (2022) 183 [2107.07395].

[54] C. Eckner, V. Vodeb, P. Martin, G. Zaharijas and F. Calore, *Detecting and characterizing pulsar haloes with the Cherenkov telescope array*, *Mon. Not. Roy. Astron. Soc.* **521** (2023) 3793 [2212.11265].

[55] T. Delahaye, J. Lavalle, R. Lineros, F. Donato and N. Fornengo, *Galactic electrons and positrons at the Earth:new estimate of the primary and secondary fluxes*, *Astron. Astrophys.* **524** (2010) A51 [1002.1910].

[56] V.M. Kaspi and D.J. Helfand, *Constraining the birth events of neutron stars*, *ASP Conf. Ser.* **271** (2002) 3 [astro-ph/0201183].

[57] M. Cirelli, G. Corcella, A. Hektor, G. Hutsi, M. Kadastik, P. Panci et al., *PPPC 4 DM ID: A Poor Particle Physicist Cookbook for Dark Matter Indirect Detection*, *JCAP* **03** (2011) 051 [1012.4515].

[58] M. Cirelli and P. Panci, *Inverse Compton constraints on the Dark Matter e+e- excesses*, *Nucl. Phys. B* **821** (2009) 399 [0904.3830].

[59] S. Vernetto and P. Lipari, *Absorption of very high energy gamma rays in the Milky Way*, *Phys. Rev. D* **94** (2016) 063009 [1608.01587].

[60] A.W. Strong, I.V. Moskalenko and V.S. Ptuskin, *Cosmic-ray propagation and interactions in the Galaxy*, *Ann. Rev. Nucl. Part. Sci.* **57** (2007) 285 [astro-ph/0701517].

[61] R. Trotta, G. Jóhannesson, I.V. Moskalenko, T.A. Porter, R.R.d. Austri and A.W. Strong, *Constraints on cosmic-ray propagation models from a global Bayesian analysis*, *Astrophys. J.* **729** (2011) 106 [1011.0037].

[62] X. Tang and T. Piran, *Positron flux and γ-ray emission from geminga pulsar and pulsar wind nebula*, *Monthly Notices of the Royal Astronomical Society* **484** (2019) 3491.

[63] G. Jó hannesson, T.A. Porter and I.V. Moskalenko, *Cosmic-ray propagation in light of the recent observation of geminga*, *The Astrophysical Journal* **879** (2019) 91.

[64] G.R. Blumenthal and R.J. Gould, *Bremsstrahlung, synchrotron radiation, and compton scattering of high-energy electrons traversing dilute gases*, *Rev. Mod. Phys.* **42** (1970) 237.

[65] F.A. Aharonian and A.M. Atoyan, *Compton Scattering of Relativistic Electrons in Compact X-Ray Sources*, *Astrophysics and Space Science* **79** (1981) 321.

[66] H.E.S.S. collaboration, *Detection of extended gamma-ray emission around the Geminga pulsar with H.E.S.S*, *Astron. Astrophys.* **673** (2023) A148 [2304.02631].

[67] CTA Consortium collaboration, *Design concepts for the Cherenkov Telescope Array CTA: An advanced facility for ground-based high-energy gamma-ray astronomy*, *Exper. Astron.* **32** (2011) 193 [1008.3703].

[68] Gammapy collaboration, *Gammapy: A Python package for gamma-ray astronomy*, 2308.13584.

[69] Fermi-LAT collaboration, *Fermi Large Area Telescope Fourth Source Catalog*, *Astrophys. J. Suppl.* **247** (2020) 33 [1902.10045].

[70] "CTAO Performance." https://www.cta-observatory.org/science/ctao-performance/.